Abdom Imaging 22:410–417 (1997)

Abdominal Imaging

Hyperintense benign liver lesions on spin-echo T1-weighted MR images: pathologic correlations

D. Mathieu,[1] **M. Paret,**[1] **A.-E. Mahfouz,**[1,*] **F. Caseiro-Alves,**[1] **J. Tran Van Nhieu,**[2] **M.-C. Anglade,**[1] **A. Rahmouni,**[1] **N. Vasile**[1]

[1]Department of Radiology, Hôpital Henri Mondor, 51 avenue du Maréchal de Lattre de Tassigny, F-94010 Créteil, France
[2]Department of Pathology, Hôpital Henri Mondor, 51 avenue du Maréchal de Lattre de Tassigny, F-94010 Créteil, France

Received: 6 February 1996/Accepted: 27 March 1996

Abstract
Background: To determine the incidence of hyperintensity on T1-weighted spin echo (SE) images in benign liver lesions, value of fat-suppressed magnetic resonance (MR) imaging for the detection of fat within these lesions, and the causes of hyperintensity by correlation to pathologic examinations.
Methods: Five hundred forty-nine patients with 805 benign liver lesions including 585 hemangiomas, 188 focal nodular hyperplasias (FNHs), 14 hepatic adenomas (HAs), 14 focal fatty infiltrations (FFIs), two biliary cystadenomas, and two hemorrhagic cysts were examined by T2-weighted and T1-weighted SE MR imaging. For hyperintense lesions on T1-weighted SE images, fat-suppressed images were obtained by selective presaturation of fat.
Results: Thirty-two lesions (four FNHs, 10 HAs, 14 FFIs, two biliary cystadenomas, and two hemorrhagic cysts) appeared hyperintense on T1-weighted SE images; 21 of these became hypointense on the fat-suppressed T1 weighted SE images (one FNH, six HAs, and 14 FFIs) and contained fat at pathological examination. The other 11 lesions remained hyperintense on fat-suppressed T1-weighted SE images and had no fat deposition. Causes of hyperintensity in these cases were sinusoidal dilatation, copper deposition, hemorrhage, and high protein content.
Conclusion: Among benign liver lesions, hyperintensity on T1-weighted SE images is rare (3.9%). Causes of this hyperintensity are fat deposition, copper accumulation, sinusoidal dilatation, hemorrhage, and high protein content. Fat-suppressed imaging can distinguish fat deposition from other causes of hyperintensity.

Key words: Magnetic resonance (MR), fat suppression—Liver, MR—Liver neoplasms.

Most benign liver lesions are hypointense or isointense on T1-weighted spin echo (SE) magnetic resonance (MR) images. Hyperintense lesions on these images form a special diagnostic category. The previous articles that surveyed the spectrum of hyperintense lesions on T1-weighted SE images have concentrated on malignant neoplasms more than on benign lesions [1, 2]. Furthermore, chemical-shift MR imaging has been used to assess the presence of intratumoral fat [2], but selective fat saturation has not, to our knowledge, been used to differentiate fat from other causes of hyperintensity in a large series of hyperintense hepatic lesions. The purpose of our study, which includes a large series of benign liver lesions, was to determine (1) frequency of high signal intensity on T1-weighted SE images in benign liver lesions, (2) value of fat-suppressed imaging for the diagnosis of fat deposition within these lesions, and (3) causes of hyperintensity by correlation of MR findings and pathologic examinations.

Subjects and methods

Subjects

The MR images of 549 consecutive patients with 805 benign liver lesions examined over a 4-year period were retrospectively reviewed for signal intensity on T1-weighted SE images. The lesions included

**Present address:* Radiology Dapartment, Cairo University Hospital, Cairo, Egypt

Correspondence to: D. Mathieu

585 hemangiomas, 188 focal nodular hyperplasias (FNHs), 14 hepatic adenomas (HAs), 14 focal fatty infiltrations (FFIs), two biliary cystadenomas, and two hemorrhagic hepatic cysts. The diagnosis was proved histologically in 83 lesions (51 FNHs, 14 HAs, 14 FFIs, two biliary cystadenomas, and two hemorrhagic cysts) and by typical imaging findings, silent clinical course, and constancy of size and appearance on imaging follow up for a period of 10 months to 3 years in all the hemangiomas and in 137 FNHs. Criteria for inclusion in the study, besides the presence of a benign liver lesion, included the absence of cirrhosis (determined by normal liver function tests and normal configuration of the liver on imaging) and absence of iron overload (determined by absence of history of hemolysis or blood transfusion and by preserved contrast between the liver and spleen on MR images).

The lesions that appeared hyperintense on T1-weighted SE images were selected for detailed image analysis. For all the hyperintense lesions on T1-weighted SE images, quantitative and qualitative analyses of the images were done, and results of the pathological examination were reviewed.

MR imaging

All patients were examined at 1.5 T (Magnetom SP 63; Siemens, Erlangen, Germany) by T2-weighted SE sequence (TR = 2200 ms, TE = 45 and 90 ms, matrix of 192 × 256, two acquisitions, 8-mm slice thickness, and 0.8-mm gap) and T1-weighted sequence (TR = 500 ms, TE = 15 ms, matrix of 192 × 256, three acquisitions, 8-mm slice thickness, and 0.8-mm gap). When hyperintensity was observed in a lesion on T1-weighted SE images, fat-suppressed technique was performed by transmitting a chemically selective radiofrequency pulse centered on the frequency of lipid resonance to drop out the fat signal. To obtain a good shim status, the liver was centered at the 0 position along the z axis; to obtain the best frequency adjustment for each patient on the lipid peak, a tune-up procedure was achieved with different values of frequency off-set.

Image analysis

Qualitative analysis

MR images of all the 549 patients were reviewed by two radiologists (D.M., A.R) in concert. The lesions that appeared hyperintense on T1-weighted SE images were assessed for signal intensity versus the signal intensity of the surrounding liver parenchyma on the fat-suppressed T1-weighted SE images; lesions were defined as hypo-, iso-, or hyperintense.

Quantitative analysis

For all lesions that appeared hyperintense on T1-weighted SE images, signal intensity of the lesion and the liver were measured on T1-weighted SE and fat-suppressed T1-weighted SE images by using operator-defined region of interest (ROI) that was placed manually over the lesion and encompassed at least 25 pixels. The ROI was placed within the most homogeneous part. The ratio of the signal difference between the lesion and surrounding liver parenchyma and noise (SD/N) was computed as follows: $SD/N = (S_{lesion} - S_{liver}/SD$ of the background noise, where S_{lesion} is the signal intensity of the lesion and S_{liver} is the signal intensity of the surrounding liver parenchyma. Noise was measured by placing the ROI anterior to the patient in the phase-encoding direction.

Pathologic study

For the pathologic study, material obtained from resection specimens and biopsies was fixed in 10% formalin and embedded in paraffin. Sections were stained with hematein-eosin-safran, picro-Sirius red technique, and the Perls method. Rhodanine stain was performed to detect intratumoral copper.

Results

Thirty-two lesions appeared hyperintense on T1-weighted SE images. These lesions included four FNHs, 10 HAs, 14 FFI, two biliary cystadenomas, and two hemorrhagic cysts. The diagnosis was histologically proved in these lesions.

Among the 585 hemangiomas, no high signal intensity was noted on T1-weighted SE images.

Among the 188 FNHs, four lesions (2.1%) were hyperintense on T1-weighted SE images. Two of these lesions were observed in the same patient (Fig. 1). On fat-suppressed T1-weighted SE images, two different patterns were observed: one of the two lesions became hypointense, whereas the other remained hyperintense. Pathological examination demonstrated, in addition to the typical features of FNH in both lesions, accumulation of fat within the hepatocytes in the lesion, which became hypointense and sinusoidal dilatation in the lesion and which remained hyperintense on fat-suppressed images (Table 1). The two remaining FNHs were hyperintense on both T1-weighted SE and fat-suppressed images. Histopathological examination revealed copper accumulation in these two FNHs. No hemorrhage was observed in any of the histologically proved FNHs. In the histologically proved FNHs that were not hyperintense on T1-weighted SE images (47 FNHs), no copper accumulation, fat deposition, or sinusoidal dilatation was observed at pathological examination.

In 10 of 14 HAs (71.4%), a high signal was observed on T1-weighted SE images. On fat-suppressed T1-weighted SE images, six of these 10 lesions became hypointense. On pathologic examination, fatty changes were present in these six lesions, associated in one case with sinusoidal dilatation. However, four HAs remained hyperintense on the fat-suppressed T1-weighted SE images. Three of these were proved to be hemorrhagic at pathologic examination (Fig. 2). These three tumors were observed in women with acute and recent right hypochondrial pain (Table 2). In the remaining tumor, pathological examination revealed an area of sinusoidal dilatation clearly separated from another area of fibrous tissue replacing previous necrosis and hemorrhage. No intratumoral copper was present on rhodanine stains in any of the HAs. In the Has that were not hyperintense on T1-weighted SE images (four HAs), no hemorrhage, fat deposition, or sinusoidal dilatation was observed. The two hemorrhagic cysts remained homogeneously hyperintense on fat-suppressed T1-weighted images

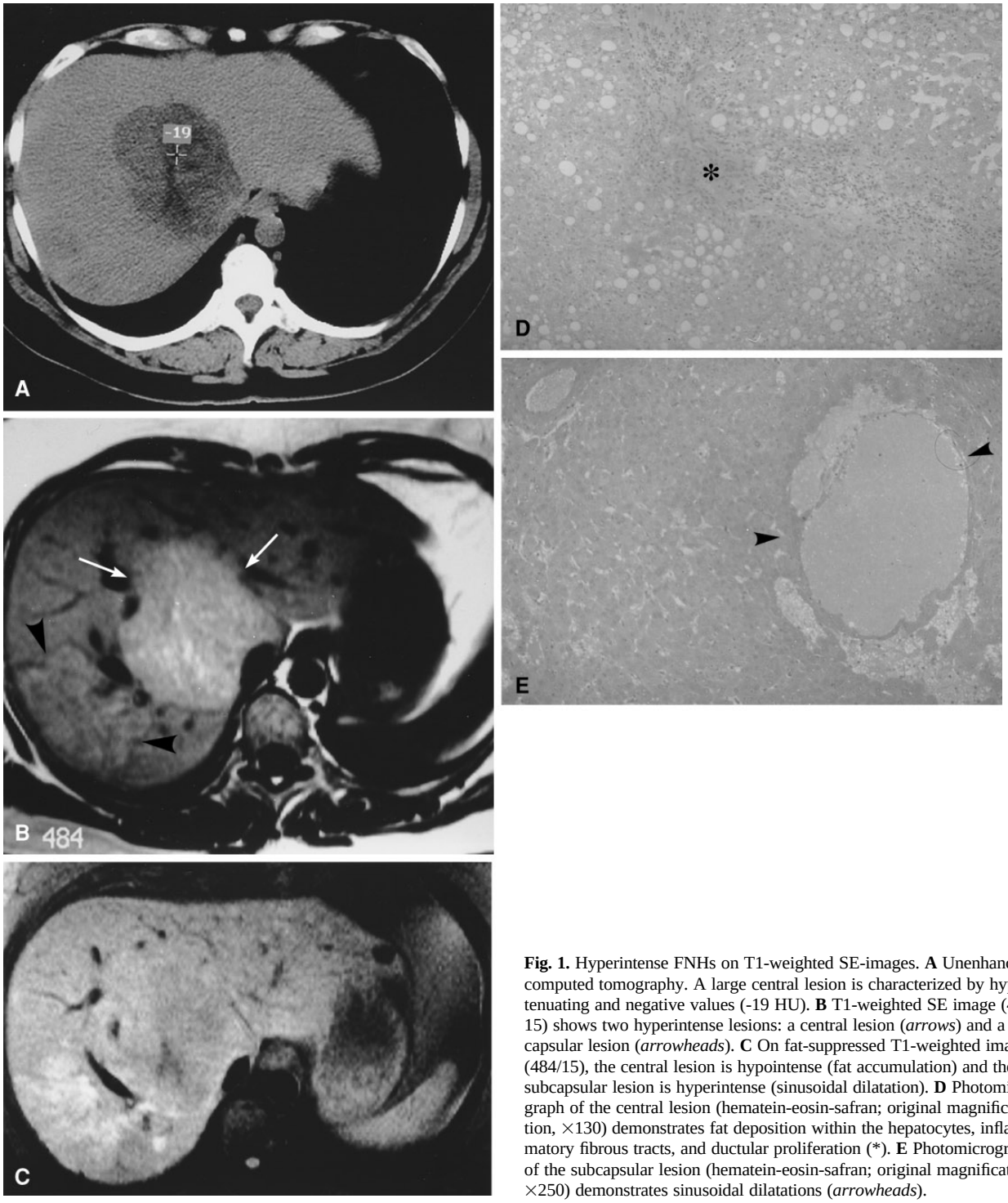

Fig. 1. Hyperintense FNHs on T1-weighted SE-images. **A** Unenhanced computed tomography. A large central lesion is characterized by hypoattenuating and negative values (-19 HU). **B** T1-weighted SE image (484/15) shows two hyperintense lesions: a central lesion (*arrows*) and a subcapsular lesion (*arrowheads*). **C** On fat-suppressed T1-weighted images (484/15), the central lesion is hypointense (fat accumulation) and the subcapsular lesion is hyperintense (sinusoidal dilatation). **D** Photomicrograph of the central lesion (hematein-eosin-safran; original magnification, ×130) demonstrates fat deposition within the hepatocytes, inflammatory fibrous tracts, and ductular proliferation (*). **E** Photomicrograph of the subcapsular lesion (hematein-eosin-safran; original magnification, ×250) demonstrates sinusoidal dilatations (*arrowheads*).

(Table 3). In both cases, macroscopic examinations showed hemorrhagic fluid within the cystic cavity. Histologically, the lesions were proved to be hepatic cysts containing numerous cells with hemosiderin deposition. The lining cells of the cysts were regular and surrounded by thick inflammatory fibrosis.

In the 14 patients with FFI, the lesion became hypointense on fat-suppressed T1-weighted SE images (Table 4). Histopathological examination demonstrated foci of hepatocytes, with intracellular fat vacuoles in all these lesions.

The two benign biliary cystadenomas remained hyperintense on fat-suppressed T1-weighted SE images.

Table 1. FNH with high signal intensity on SE T1-weighted images (n = 4): pathological findings and SD/Ns (mean ± SD) for three pulse sequences

Lesions	Pathology	SE T1-weighted	Fat-suppressed SE T1-weighted	SE T2-weighted (TE = 90 ms)
1	Fatty infiltration	6.1 ± 2.1	−3.3 ± 1.8	8.0 ± 2.6
1	Sinusoidal dilatation	1.8 ± 0.5	4.0 ± 1.8	6.6 ± 2.3
1	Copper accumulation	4.8 ± 0.7	7.2 ± 0.5	7.8 ± 0.5
1	Copper accumulation	3.8 ± 0.5	5.4 ± 1.5	7.6 ± 2.3

Table 2. Hepatocellular adenoma with high signal intensity on SE T1-weighted images (n = 10): pathological findings and SD/Ns (mean ± SD) for three pulse sequences

Lesions	Pathology	SE T1-weighted	Fat-suppressed SE T1-weighted	SE T2-weighted (TE = 90 ms)
5	Fatty infiltration	15.1 ± 3.6	−12.8 ± 4.0	4.4 ± 2.1
1	Fatty infiltration and sinusoidal dilatation	6.5 ± 2.6	−7.7 ± 2.8	2.2 ± 1.1
3	Hemorrhage[a]	17.5 ± 3.5	28.3 ± 4.0	68.7 ± 8.4
1	Sinusoidal dilatation	5.6 ± 1.6	8.1 ± 2.1	1.7 ± 0.8

[a] These three lesions occurred in women with acute right hypochondrial pain, respectively, 2 months, 3 weeks, and 1 week before MR examination

Table 3. Hemorrhagic cyst with high signal intensity on SE T1-weighted images (n = 2): pathological findings and SD/Ns (mean ± SD) for three pulse sequences

Lesions	Pathology	SE T1-weighted	Fat-suppressed SE T1-weighted	SE T2-weighted (TE = 90 ms)
1	Hemorrhage	21.3 ± 2.5	30.3 ± 4.0	92.7 ± 2.4
1	Hemorrhagic	15.6 ± 1.6	24.1 ± 2.0	70.7 ± 1.8

In one of these cases, pathological examination revealed a cystic lesion with mucinous content lined by a single layer of benign PAS-positive cubocolumnar epithelial cells and surrounded by fibrous tissue. In the other case, pathological examination revealed a cystic lesion containing hemorrhagic fluid lined by nonmucinous (PAS-negative) benign epithelial cells with papillary projections.

Among the 32 lesions that appeared hyperintense on the T1-weighted SE images, 21 lesions appeared hypointense on the fat-suppressed T1-weighted SE images (one FNH, six HAs, and 14 FFIs). Pathological examination confirmed the presence of excessive fat deposition in all these lesions (Fig. 3), associated in one of the HAs with sinusoidal dilatation (Fig. 4). In the remaining 11 lesions, which remained hyperintense on fat-suppressed T1-weighted SE images, no excessive fat deposition was observed at pathological examination (Figs. 5, 6). The pathological features in these cases were sinusoidal dilatation in two lesions (one FNH and one HA), copper deposition in two FNHs, hemorrhage in six lesions (three HAs, two hemorrhagic cysts, and one biliary cystadenoma), and high protein content in one biliary cystadenoma.

Discussion

The demonstration of a high signal intensity in benign liver tumors is rather rare and was observed in 32 of the 805 lesions of our series (3.9%). However, our study did not include cases of benign liver lesions in cases of cirrhosis or hepatic iron overload, which excludes the regenerative nodules that are notorious for their malignant potential and that may appear hyperintense on T1-weighted SE images [3, 4]. This study also excludes benign lesions that may occur in cases of hepatic iron overload. Such lesions would appear hyperintense due to the extremely low signal intensity of the liver and not due to their own high signal intensity.

Our results confirm that hemangioma showed no hyperintensity on T1-weighted SE images. To our knowledge, hyperintensity of hemangioma on T1-weighted SE images has never been reported in the literature.

Our results showed that hyperintensity of benign hepatic lesions on T1-weighted images can be due to different pathological changes including fat deposition, copper accumulation, high protein concentration, blood degradation products, or sinusoidal dilatation. The mechanism by which hyperintensity occurs is different

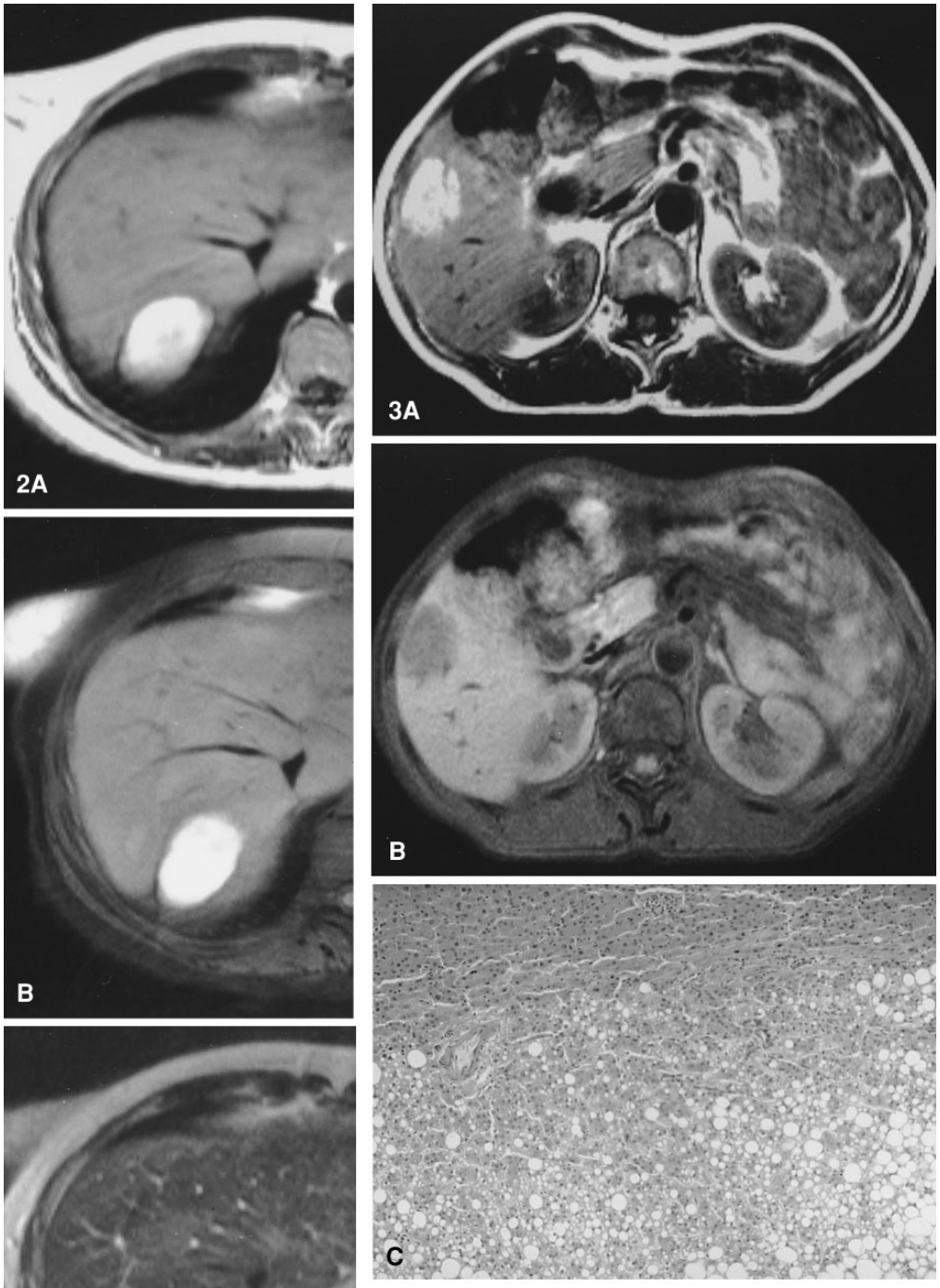

Fig. 2. Hepatocellular adenoma with hemorrhage. Hyperintense subcapsular lesion is shown on all sequences. **A** T1-weighted SE image (420/15). **B** Fat-suppressed T1-weighted images (420/15). **C** T2-weighted SE image (2200/90). A hypointense rim is seen around the lesion, denoting hemosiderin deposition.

Fig. 3. Hepatocellular adenoma with fat accumulation. **A** T1-weighted SE image (420/15). The lesion is hyperintense. **B** Fat-suppressed T1-weighted images (420/15). The lesion is hypointense. **C** Pathologic examination of the resected tumor. The difference between the normal liver (upper) and the liver cell adenoma, which demonstrates macrovesicular and microvesicular fat deposition (lower), is obvious. Compressing liver parenchyma is seen in between the normal liver and the liver cell adenoma (hematein-eosin-safran; original magnification, ×130).

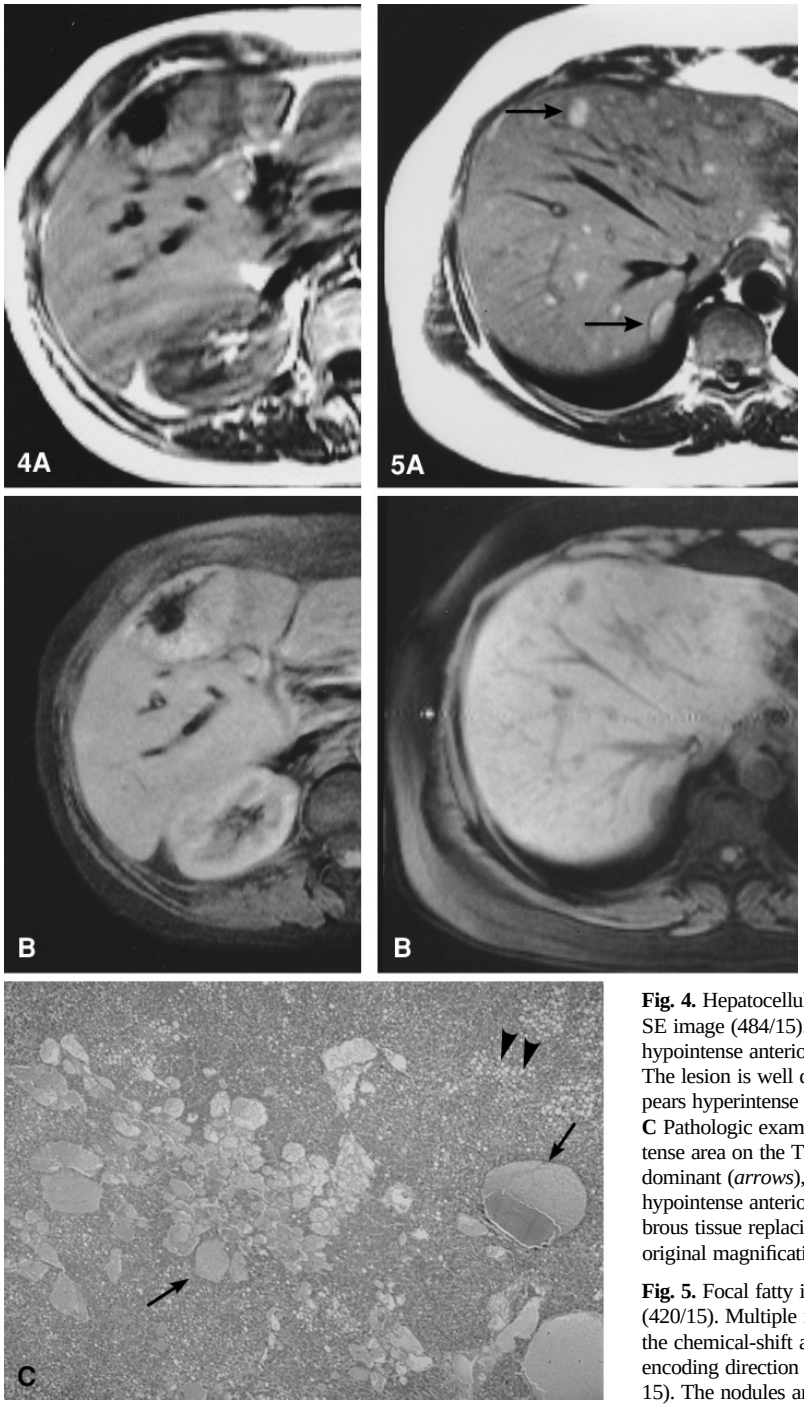

Fig. 4. Hepatocellular adenoma with sinusoidal dilatation. **A** T1-weighted SE image (484/15). The lesion is hyperintense relative to the liver, with a hypointense anterior area. **B** Fat-suppressed T1-weighted images (484/15). The lesion is well demarcated from the surrounding parenchyma and appears hyperintense relative to the liver, with a hypointense anterior area. **C** Pathologic examination of the resected tumor. In the posterior hyperintense area on the T1-weighted SE image, a sinusoidal dilatation was predominant (*arrows*), combined with fatty deposition (*arrowheads*). The hypointense anterior area on SE T1-weighted images corresponded to a fibrous tissue replacing the previous hemorrhage (hematein-eosin-safran; original magnification, ×32).

Fig. 5. Focal fatty infiltration, multinodular form. **A** T1-weighted SE image (420/15). Multiple nodules appear hyperintense relative to the liver. Notice the chemical-shift artifact, present close to the fatty areas, in the frequency-encoding direction (*arrows*). **B** Fat-suppressed T1-weighted images (420/15). The nodules are hypointense relative to liver.

in these different situations. Fat deposition has high signal due to its short T1. Copper causes high signal due to its paramagnetic effect [5]. High protein concentration causes high signal due to the bound water content within the macromolecular proteins. The signal intensity of hematoma depends on its age; its high signal is attributed to the paramagnetic effect of methemoglobin and the increase in protein concentration caused by the increase in number of red blood cells per unit volume [6]. The mechanism by which sinusoidal dilatation causes high signal on T1-weighted images is not fully understood. Sinusoidal dilatation occurs in HA, particularly in women who use oral contraceptives. Arrivé et al. demonstrated this dilatation in 17 of 30 hyperintense lesions on T1-weighted SE images [7]; Vilgrain et al. also demonstrated this in two FNH lesions [8]. A pos-

Table 4. FFI with high signal intensity on SE T1-weighted images (n = 14): pathological findings and SD/Ns (mean ± SD) for three pulse sequences

Patients	Pathology	SE T1-weighted	Fat-suppressed SE T1-weighted	SE T2-weighted (TE = 90 ms)
14	Focal fatty infiltration	7.4 ± 2.3	−14.4 ± 3.8	1.8 ± 0.8

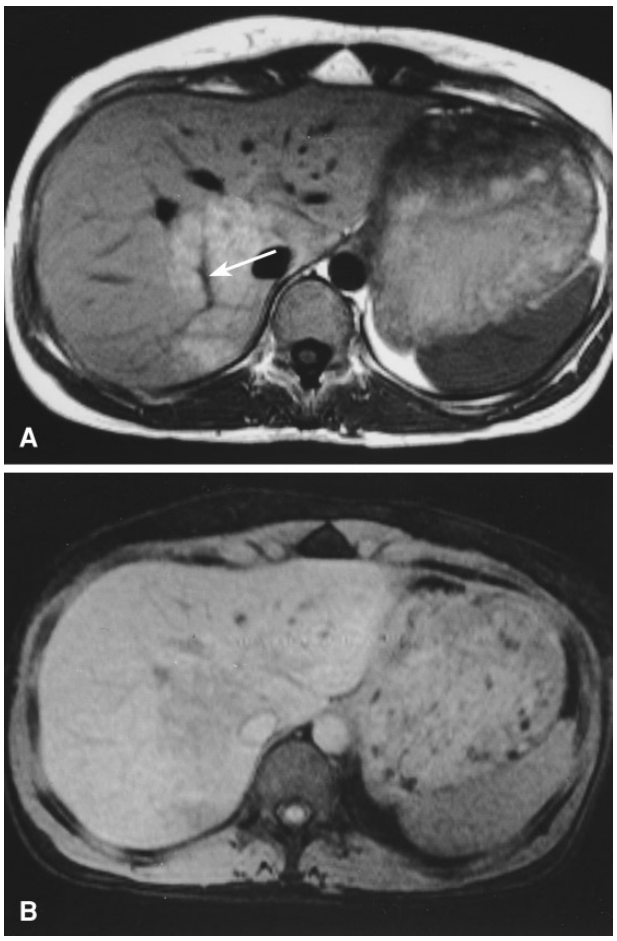

Fig. 6. Focal fatty infiltration, infiltrative form. **A** T1-weighted SE image (420/15). Large area is hyperintense relative to the liver. Note the portal vessel within this area (*arrow*). **B** Fat-suppressed T1-weighted images (420/15). The area is hypointense relative to the liver.

sible explanation for the hyperintensity of the lesions with sinusoidal dilatation might be the slow flow of blood, which results in an increase of its viscosity or the possible associated thrombosis.

In our study, hyperintensity of FNH on T1-weighted SE images was due to fat deposition, copper accumulation, or sinusoidal dilatation. In six previously published series of FNH, including 153 lesions examined at different field strengths varying from 0.35 T to 2 T, five lesions (3.3%) have been described as hyperintense on SE T1-weighted images [8–13]. Pathological study was available in four of these five FNHs. Hyperintensity was explained by intralesional hemorrhage in one case [10] and by sinusoidal dilatation in two FNHs [8]. In one FNH, no explanation for hyperintensity was found at pathological examination [8]. Furthermore, Mitchell et al. reported a single FNH, which was hyperintense on T1-weighted SE images [2]. This lesion demonstrated intralesional fatty infiltration; however, this FNH occurred in a fatty liver, and the intralesional fat deposition was explained as an exaggerated expression of the patient's native pathology [2]. Copper accumulation has been described as a cause of hyperintensity on T1-weighted SE images in hepatocellular carcinoma [5]. However, to our knowledge, hyperintensity due to accumulation of copper within FNH has not been previously reported. Copper accumulation occurs in association with cholestasis in primary biliary cirrhosis [14]. Because cholestatic features such as canalicular bile plugs can also occur in FNH [15], we attribute copper accumulation in our two FNH lesions to cholestasis. However, there should be some other contributing factors because cholestatic features are relatively common within FNH, whereas copper accumulation is quite rare.

In comparison with FNH, HAs have a striking tendency to be hyperintense on T1-weighted images. Different studies and isolated case reports have emphasized that hyperintensity and heterogeneity of these tumors can be related to fatty deposition or hemorrhage [7, 16–22]. This high signal intensity relative to the liver has been observed in 10 of our 14 HA lesions (71.5%). These results confirm the recent data published by Paulson et al., which demonstrated a high signal intensity in 51 (77%) of 66 HAs observed in 14 patients [17], and those reported by Arrivé et al., which demonstrated a high signal intensity in 30 (59%) of 51 HAs observed in 29 patients [7]. In our study, hyperintensity of HA could be attributed to fat deposition in five lesions, to combined fat deposition and sinusoidal dilatation in one lesion, to hemorrhage in three lesions, and to sinusoidal dilatation in one lesion.

Focal fatty infiltration can assume a variety of appearances, ranging from the involvement of only a small area of the liver to involvement of the entire liver with only small areas of spared normal hepatic parenchyma. In rare presentations (e.g., nodular, patchy, or irregular areas), it can be difficult to distinguish FFI from malignant lesions.

Our results show that fat saturation is sensitive for the detection of fat deposition in hyperintense lesions on T1-weighted SE images. All the hyperintense lesions that became hypointense on fat-suppressed images were proved to have fat deposition at pathological examination, whereas none of the lesions that remained hyperintense on those images showed excessive fat deposition. Furthermore, all the lesions that were shown to have fat on the fat-suppressed images were built up of hepatocytes. Thus, fat-suppressed imaging would be clinically valuable by narrowing the differential diagnosis of the hyperintense lesions to those lesions that are composed of hepatocytes. A very rare exception would be the lipomatous tumors and hamartomatous lesions of the liver such as lipomas, myolipomas, and angiomyolipomas [23].

Hyperintensity on T1-weighted SE images can also be observed in malignant liver tumors, including melanoma metastases and primary hepatocellular carcinoma [1, 2, 24]. In addition to fat deposition, high signal intensity of hepatocellular carcinoma on T1-weighted images can be explained by hemorrhage, necrotic cavities containing proteinous material, or copper deposition [5, 25–27]. For small hepatocellular carcinomas, less than 3 cm in diameter, the frequency of a high signal intensity varied from 31% to 41% and was observed particularly in clear cell tumors [25–27]. This frequency drops to 24% for lesions more than 3 cm in diameter [27]. Considering that hyperintensity on T1-weighted SE images can occur in malignant and in benign focal hepatic lesions, biopsy or surgery may be required to differentiate these tumors [28].

References

1. Lee MJ, Hahn PF, Saini S, et al. Differential diagnosis of hyperintense liver lesions on T1-weighted MR images. *AJR* 1992; 159:1017–1020
2. Mitchell DG, Palazzo J, Hann H-WYL, et al. Hepatocellular tumors with high signal on T1-weighted MR images: chemical shift and histologic correlation. *J Comput Assist Tomogr* 1991;15: 762–769
3. Koslow SA, Davis PL, De Marino GB, et al. Hyperintense cirrhotic nodules on MRI. *Gastrointest Radiol* 1991;16:339–341
4. Matsui O, Kadoya M, Kameyama J, et al. Adenomatous hyperplastic nodules in the cirrhotic liver: differentiation from hepatocellular carcinoma with MR imaging. *Radiology* 1989;173: 123–126
5. Ebara M, Watanabe S, Kita K, et al. MR imaging of small hepatocellular carcinoma: effect of intratumoral copper content on signal intensity. *Radiology* 1991;180:617–621
6. Hayman LA, Taber KH, Ford JJ, et al. Mechanisms of MR signal alteration by acute intracerebral blood: old concepts and new theories. *Am J Neuroradiol* 1991;12:899–907
7. Arrivé L, Fléjou J-F, Vilgrain V, et al. Hepatic adenoma: MR findings in 51 pathologically proved lesions. *Radiology* 1994; 193:507–512
8. Vilgrain V, Fléjou J-F, Arrivé L, et al. Focal nodular hyperplasia of the liver: MR imaging and pathologic correlation in 37 patients. *Radiology* 1992;184:699–703
9. Mathieu D, Rahmouni A, Anglade M-C, et al. Focal nodular hyperplasia of the liver: assessment with contrast-enhanced TurboFLASH MR imaging. *Radiology* 1991;180:25–30
10. Lee MJ, Saini S, Hamm B, et al. Focal nodular hyperplasia of the liver: MR findings in 35 proved cases. *AJR* 1991;156:317–320
11. Shamsi K, de Schepper A, Degryse H, et al. Focal nodular hyperplasia of the liver. *Abdom Imaging* 1993;18:32–38
12. Mattison GR, Glazer GM, Quint LE, et al. MR imaging of hepatic focal nodular hyperplasia: characterization and distinction from primary malignant hepatic tumors. *AJR* 1987;148:711–715
13. Mahfouz A-E, Hamm B, Taupitz M, et al. Hypervascular liver lesions: differentiation of focal nodular hyperplasia from malignant tumors with dynamic Gadolinium-enhanced MR imaging. *Radiology* 1993;186:133–138
14. Kowdley KV, Knox TA, Kaplan MM. Hepatic copper content is normal in early primary biliary cirrhosis and primary sclerosing cholangitis. *Dig Dis Sci* 1994;39:2416–2420
15. Butron Villa MM, Haot J, Desment VJ. Cholestatic features in focal nodular hyperplasia of the liver. *Liver* 1984;4:387–395
16. Rummeny E, Weissleder R, Stark DD, et al. Primary liver tumors: diagnosis by MR imaging. *AJR* 1989;152:63–72
17. Paulson EK, McClellan JS, Washington K, et al. Hepatic adenoma: MR characteristics and correlation with pathologic findings. *AJR* 1994;163:113–116
18. Stoupis C, Ros PR, Vilamosa JC, et al. Hepatocellular adenoma: correlation of MR imaging and pathologic findings [Abstract]. *Radiology* 1993;189(P):282
19. Chung KY, Mathieu D, Mayo-Smith WW, et al. MR imaging of hepatic adenoma: radiologic–pathologic correlation in 31 tumors [Abstract]. *Radiology* 1993;189(P):425
20. Gabata T, Matsui O, Kadoya M, et al. MR imaging of the hepatic adenoma. *AJR* 1990;155:1009–1011
21. Coombs RJ, Woldenberg LS, Skeel RT, et al. Magnetic resonance imaging of hepatic adenoma. *Clin Imaging* 1990;14:44–47
22. Choi BI, Han JK, Kim SH, et al. MR findings in liver adenomatosis. *Gastrointest Radiol* 1991;16:234–236
23. Fobbe F, Hamm B, Schwarting R. Angiomyolipoma of the liver: CT, MR and ultrasound imaging. *J Comput Assist Tomogr* 1988;12:658–659
24. Yoshikawa J, Matsui O, Takashima T, et al. Fatty metamorphosis in hepatocellular carcinoma: radiologic features in 10 cases. *AJR* 1988;151:717–720
25. Ebara M, Ohto M, Watanabe S, et al. Diagnosis of small hepatocellular carcinoma: correlation of MR imaging and tumor histologic studies. *Radiology* 1986;159:371–377
26. Itoh K, Nishimura K, Togashi K, et al. Hepatocellular carcinoma: MR imaging. *Radiology* 1987;164:21–25
27. Kadoya M, Matsui O, Takashima T, et al. Hepatocellular carcinoma: correlation of MR imaging and histopathologic findings. *Radiology* 1992;183:819–825
28. Belghiti J, Pateron D, Panis Y, et al. Resection of presumed benign liver tumours. *Br J Surg* 1993;80:380–383